Mathematical Modeling in Neuroendocrinology

Richard Bertram[*1]

ABSTRACT

Mathematical models are commonly used in neuroscience, both as tools for integrating data and as devices for designing new experiments that test model predictions. The wide range of relevant spatial and temporal scales in the neuroendocrine system makes neuroendocrinology a branch of neuroscience with great potential for modeling. This article provides an overview of concepts that are useful for understanding mathematical models of the neuroendocrine system, as well as design principles that have been illuminated through the use of mathematical models. These principles are found over and over again in cellular dynamics, and serve as building blocks for understanding some of the complex temporal dynamics that are exhibited throughout the neuroendocrine system.
© 2015 American Physiological Society. *Compr Physiol* 5:911-927, 2015.

Introduction

In 1952, Alan Hodgkin and Andrew Huxley published an article that was key to the development of modern neuroscience (22). This article demonstrated how voltage-dependent Na^+ and K^+ ion channels can work together to generate electrical impulses, and how these can travel down an axon without attenuation. This demonstration would not have been possible without the mathematical model that they developed to integrate their voltage-clamp data into a time-dependent description of the membrane potential in the squid giant axon. Indeed, the Hodgkin-Huxley model is almost certainly the most cited mathematical model in all of physiology, and is a ubiquitous topic in graduate courses on biomathematics as well as neuroscience. Many subsequent neural models use a *Hodgkin-Huxley formalism*, which means that the models use similar design principles, but somewhat different equations. Such a formalism has been employed in models of the neuroendocrine system, including models of vasopressin neurons (28,53,54), gonadotropin-releasing hormone (GnRH) neurons (12, 17, 29, 30), and pituitary gonadotrophs (33, 36, 37, 75), somatotrophs (72), corticotrophs (38), and lactotrophs (66, 67).

A major advantage of Hodgkin-Huxley-type models is their reliance on ionic currents, which can in some cases be calibrated with the use of pharmacological agents and voltage clamp (21). With an ionic current-based model one can make predictions about the effects of neuromodulators or pharmaceutical drugs, which often target ion channels through the actions of G proteins. A major disadvantage of Hodgkin-Huxley-type models is their reliance on ionic currents, which may not be well described in the cell that is being studied, or which may be seen as superfluous in studies focused on network behavior. Another class of model, the *integrate-and-fire model*, was developed to capture the threshold behavior of neurons or other electrically excitable cells, without the complexity of detailed ionic currents (23). This type of model has been used, for example, in models of oxytocin and vasopressin neurons (44, 45, 55).

The concept that "simpler is better" that underlies the use of integrate-and-fire models also underlies *functional models* (32) or *mean field models*. These describe the activity of a population of cells with a single variable. Interacting cell populations then require several interacting variables. The alternative, using a set of variables for each cell in each population, quickly gets out of hand in systems consisting of thousands or even millions of cells. Functional models have been used to describe the menstrual cycle (6, 58, 84), follicular selection (8), luteinizing hormone secretion (56), circadian surges of prolactin secretion (2), and ultradian rhythms in cortisol secretion (82) and growth hormone secretion (43).

An aim of this article is to provide an overview of some of the key mathematical concepts that are used in models of the types described above. Many of these concepts are intuitive, and can be understood without the background (calculus, linear algebra, linear, and nonlinear differential equations) typical of the mathematical modelers who generate the models. Another aim is to identify design principles that underlie models across cell types. Understanding these principles facilitates understanding of some of the complex dynamics that occur throughout the neuroendocrine system. We omit discussion of many mathematical and numerical issues involved in analyzing the different types of mathematical models. A nice discussion of nonlinear ordinary differential equations (ODEs) can be found in (65), while discussion of both ordinary and partial

[*]Correspondence to bertram@math.fsu.edu

[1]Department of Mathematics, and Programs in Neuroscience and Molecular Biophysics, Florida State University, Tallahassee, Florida, USA

Published online, April 2015 (*comprehensivephysiology.com*)

DOI: 10.1002/cphy.c140034

Copyright © American Physiological Society.

differential equations (PDEs) and their application to physiology can be found in (24, 25). Delay differential equations (DDEs) are discussed in detail in (15). Finally, numerical methods for solving the different types of equation can be found in (50).

Getting Started

We begin by addressing basic questions that a neuroendocrinologist may ask when evaluating modeling studies or when considering whether to incorporate modeling into his/her own research.

Why use mathematical models?

The neuroendocrine system is extraordinarily complex, due largely to the many interactions of its constituent parts. The complexity is reduced somewhat by formally partitioning the system into "axes," such as the hypothalamus-pituitary-adrenal axis, or *stress axis*. To further simplify, one often focuses on one physiological state, or on one cell type (e.g., the corticotroph). This reductionist approach has proven to be very successful and our understanding of the components of the full system has blossomed over the past few decades. Ultimately, though, one must tie the pieces together to generate a larger picture. This integration occurs at all levels and is most often represented with *box-and-arrow diagrams*, which illustrate how one factor acts on another. *A mathematical model converts box-and-arrow diagrams into equations*. This is demonstrated in Figure 1, which shows two interacting elements (these could be cell populations, individual cells, or signaling molecules). Element A stimulates B, while B inhibits A. The box-and-arrow diagram could be the "model" that results from a thorough study of these two elements. However, one could go further, by writing equations such as the following for the dynamics of A and B:

$$\frac{dA}{dt} = p_1 - p_2\frac{B}{K_B + B} - p_3 A \quad (1)$$

$$\frac{dB}{dt} = p_4 + p_5\frac{A}{K_A + A} - p_6 B \quad (2)$$

where the inhibitory effect of B on A is through the p_2 term and the stimulatory effect of A on B through the p_5 term. We immediately recognize that a problem has emerged; one must now provide values for the eight parameters p_1 to p_6, K_A, and K_B. That is, the mere act of writing down

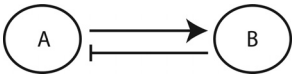

Figure 1 Box-and-arrow diagram indicating that A stimulates B and B inhibits A.

equations forces one to consider not just how the two elements are interacting, but the strength of their interactions (parameters p_2, K_B, p_5, and K_A) in the context of the intrinsic dynamics of A and B (set by p_1, p_3, p_4, and p_6). The need to find values for these parameters, that is, to calibrate the model, could motivate additional experiments. A question that arises when going from Figure 1 to Eqs. 1 and 2 is whether the interactions are both rapid or whether one pathway is slow relative to the other and relative to the intrinsic dynamics of A and B. For example, if the inhibitory influence of B onto A is slow, then sustained oscillations in A and B can be produced. How slow or delayed must this inhibitory influence be to produce oscillations? What is the period of the oscillations? How does it depend on the delay or speed in inhibition? These questions cannot be answered using the box-and-arrow diagram, but they are readily accessible through mathematical analysis and computer simulations of the mathematical model.

Is bigger better?

Evolution and natural selection have an excellent track record for solving problems. Unfortunately, the solutions obtained through this process are rarely the simplest, at least in the eyes of an engineer. It is, therefore, often the case that many interacting elements combine to produce a behavior that could just as easily have been produced with two or three key elements. For example, elements C, D, E, and F may all act on A, and G, H, I, J, and K, may act on B. Should one include these extra elements in the mathematical model? That is, is bigger better? There are several reasons for including everything. The most obvious is that each interaction likely took a lot of work to uncover, so it surely deserves to be included in the model. Another is that if the element is a part of the biological system, and even if it appears to be a minor player in the production of the behavior of interest, it may play a major role in some other behavior that may studied later. Frontloading the model with all the known elements ensures that everything will be there when needed. In addition, elements that appear to be bit players may be targets of physiological modulators or pharmacological agents, and would have to be in the model if one is to study these things. So in some ways bigger is better.

Other arguments can be made that lead one to quite a different conclusion. Perhaps the most compelling argument against big mathematical models is that the larger the model the harder it is to understand. Mathematical tools are excellent for understanding dynamic models with a few dependent variables. That is, models with a low-dimensional *state space*. Their utility drops off quickly at higher dimensions. For higher dimensional systems the primary tool is computer simulation. With modern computers, it is entirely possible to do simulations of more than a hundred dynamic equations on a desktop computer, and many more on supercomputers or with graphics processing units. But there is another problem: as the dimensionality of the model grows so too does the

number of parameters. That is, the dimensionality of *parameter space* is typically larger with larger models. Since most parameters will be known only to within some range of values, this means that to understand the range of behaviors that can be exhibited by the model one must do simulations over a large set of sample points in parameter space. Such a *parameter exploration* can quickly become intractable, and one will be left with a very incomplete understanding of the model. If Hodgkin and Huxley had studied the soma of a neuron, which contains many types of ion channels, rather than the axon that expresses only two voltage-dependent channels, would their model have led them to the fundamental insights that they achieved through simulations with their "simple" four-dimensional model? Probably not. Indeed, simpler is usually better for understanding how a system works. A successful strategy then is to start simple and take advantage of the low dimensionality of the state space and parameter space to gain insights into the dynamics of the fundamental elements of the system. This can be followed by the addition of new elements as suggested by the data and by the questions that one wishes to answer. So at least at first, simpler is often better.

Types of Equations

The focus of this article is on *dynamic models*, that is, models that describe how a system changes over time. In this section, we discuss the several types of equations that are most frequently encountered in physiological dynamic models.

Ordinary differential equations

These are the types of equations encountered in calculus and basic physics classes, and famously describe the motion of falling objects and celestial bodies. An ODE like Eq. 1 simply describes how a dependent variable, A in this case, changes over a small time increment. The right hand side of the equation can therefore be thought of as the instantaneous speed of A, which may be positive (A is increasing), negative (A is decreasing), or zero (A is at rest). If the speed is a linear function of the dependent variables, then the ODE is *linear*. Formulas exist for the solution of linear ODEs. Unfortunately, most physiological models consist of nonlinear ODEs, and solution formulas typically do not exist, so one is compelled to approximate the solution using a computer. Equation 1 is a nonlinear ODE that is also coupled to the dependent variable B. Indeed, the nonlinearity comes in through the coupling term, which has an increasing and saturating dependence on B (this is called a *Michaelis-Menten function*). Since Eq. 1 contains a first derivative and no higher order derivatives, it is a *first-order ODE*. In contrast, Newton's equation of motion ($F = ma$) contains a second derivative for acceleration, and is a *second-order ODE*.

The Hodgkin-Huxley model is described in terms of a system of nonlinear first-order ODEs:

$$C_{\mathrm{m}}\frac{\mathrm{d}V}{\mathrm{d}t} = I_{\mathrm{app}} - I_{\mathrm{Na}} - I_{\mathrm{K}} - I_l \tag{3}$$

$$\frac{\mathrm{d}m}{\mathrm{d}t} = \frac{m_\infty(V) - m}{\tau_m(V)} \tag{4}$$

$$\frac{\mathrm{d}n}{\mathrm{d}t} = \frac{n_\infty(V) - n}{\tau_n(V)} \tag{5}$$

$$\frac{\mathrm{d}h}{\mathrm{d}t} = \frac{h_\infty(V) - h}{\tau_h(V)} \tag{6}$$

The first equation, Eq. 3, says that the membrane capacitance, C_{m}, times the time derivative of the membrane potential, V, is equal to the sum/difference of the ionic currents. This appears to be quite simple, and indeed the ionic currents are all described by Ohm's law, which depends linearly on the voltage: $I_{\mathrm{Na}} = g_{\mathrm{Na}}\left(V - V_{\mathrm{Na}}\right)$. Is the voltage equation a simple linear ODE? If it were, then action potentials would not occur and we'd all be dead. Fortunately for us, the Na^+ and K^+ conductances, g_{Na} and g_{K}, vary over time as described by the dynamics of gating variables, and this makes the system nonlinear. This was one of the great discoveries of Hodgkin and Huxley, and is at the heart of electrical excitability. The other ODEs in the Hodgkin-Huxley model describe how the gating variables change over time: m and h are the Na^+ activation and inactivation variables, respectively, and n is the K^+ activation variable. Each of these satisfies *first-order kinetics*, for example, the variable m approaches its equilibrium m_∞ exponentially with a rate determined by the "time constant" τ_m. If the time constant is large, then the approach to equilibrium is slow. Adding to the complexity, and making the whole thing work, is the fact that both the equilibrium and the time constant are voltage dependent (so "time constant" is a misnomer). Finally, the Na^+ and K^+ currents can be written as:

$$I_{\mathrm{Na}} = \bar{g}_{\mathrm{Na}} m^3 h\left(V - V_{\mathrm{Na}}\right) \tag{7}$$

$$I_{\mathrm{K}} = \bar{g}_{\mathrm{K}} n^4\left(V - V_{\mathrm{K}}\right) \tag{8}$$

where $\bar{g}$ is the conductance when the channel is maximally activated (and not inactivated). The currents, and thus the voltage ODE, are now clearly nonlinear. The equilibrium or "infinity functions" and the time constant functions are written in terms of the forward and backward transition rates: $m_\infty(V) = \alpha_m/(\alpha_m + \beta_m)$, $n_\infty(V) = \alpha_n/(\alpha_n + \beta_n)$, $h_\infty(V) = \alpha_h/(\alpha_h + \beta_h)$, and $\tau_m(V) = 1/(\alpha_m + \beta_m)$, $\tau_n(V) = 1/(\alpha_n + \beta_n)$, and $\tau_h(V/(\alpha_h + \beta_h)$. The α and β functions, as well as parameter values for the models used in the figures, are given in Table 1.

Delay differential equations

In Eq. 1, the change of A at a particular time depends partly on the value of B at that time. What if, instead, it depended

Table 1 Parameter Values and Functions for Models Used to Make the Figures

Hodgkin-Huxley model (Eqs. 3-6, 24, and 25)			
$C_m = 1\ \mu F/cm^2$	$\bar{g}_{Na} = 120\ mS/cm^2$	$\bar{g}_K = 36\ mS/cm^2$	$\bar{g}_l = 0.3\ mS/cm^2$
$V_{Na} = 50\ mV$	$V_K = -75\ mV$	$V_l = -50\ mV$	$I_{ap} = 0, 1, 1.5\ \mu A/cm^2$
$\alpha_m = \frac{0.1\,(V+40)}{1-e^{-(V+40)/10}}$	$\beta_m = 4\,e^{-(V+65)/18}$	$\alpha_n = \frac{0.01\,(V+55)}{1-e^{-(V+55)/10}}$	$\beta_n = 0.13\,e^{-(V+65)/80}$
$\alpha_h = 0.07e^{-(V+65)/20}$	$\beta_h = \frac{1}{1+e^{-(V+30)/10}}$	$I_{noise}^{max} = 0.3\ \mu A/cm^2$	
Genetic toggle switch (Eqs. 18 and 19)			
$\alpha_x = 10, 9$	$\alpha_y = 10$	$\beta = 2, 1.5, 1$	$\gamma = 2, 1.5, 1$
$p_5 = 0.11$	$p_6 = 2.9$		
Prolactin model (Eqs. 22 and 23)			
$T_p = 6$	$q = 0.5$	$T_d = 10$	$k_p = 0.03$
$\tau = 0.5, 1.5, 3\ h$			
Relaxation oscillator (Eqs. 26 and 27)			
$p_1 = 0.1$	$p_2 = 0.5$	$\varepsilon = 1, 0.05$	
Bursting "s" model (Eqs. 28-30)			
$C_m = 4524\ fF$	$\bar{g}_{Ca} = 280\ pS$	$\bar{g}_K = 1300\ pS$	$\bar{g}_{K(ATP)} = 13\ pS$
$\bar{g}_L = 25\ pS$	$\bar{g}_{Ks} = 20\ pS$	$V_{Ca} = 100\ mV$	$V_K = -80\ mV$
$V_L = -40\ mV$	$\tau_s = 10,000\ ms$	$m_\infty = \frac{1}{1+e^{-(22+V)/7.5}}$	$n_\infty = \frac{1}{1+e^{-(9+V)/10}}$
$s_\infty = \frac{1}{1+e^{-(40+V)/0.5}}$	$\tau_n = \frac{8.26}{1+e^{(V+9)/10}}$		

on B at an earlier time? Then the equation would be a DDE. One can easily imagine situations where DDEs may be used. For example, the rate at which the protein level for some gene product changes depends on the mRNA level for that protein some time earlier, since translation takes time. Whether or not one includes the time delay in the model is determined partly by how important it is thought to be. In terms of Figure 1, if the inhibition of A by B were delayed by τ time units, then Eq. 1 would become the following DDE:

$$\frac{dA}{dt} = p_1 - p_2\frac{B_\tau}{K_B + B_\tau} - p_3 A \tag{9}$$

where B_τ means B evaluated at time $t - \tau$.

A DDE was used recently to describe ultradian (hourly) oscillations in glucocorticoid (CORT) levels in the blood (82). Experimental studies indicated that these oscillations are not due to oscillatory levels in corticotropin-releasing hormone (CRH) from the hypothalamus, and in fact the CORT oscillations persisted in rats in which the CRH level was constant (81). The explanation given was that mutual interactions between pituitary corticotrophs and CORT-releasing cells in the adrenal cortex are responsible for the rhythm. That is, corticotrophs release corticotropin (ACTH) that stimulates the production and release of CORT from adrenal cortex cells. The CORT then has an inhibitory effect on the corticotrophs. So this is just Figure 1 again, with A being the release of ACTH and B the release of CORT. Because the CORT is not stored, but must be synthesized when signaled by the ACTH, there is a time delay in the release of CORT. The model equations are:

$$\frac{da}{dt} = \frac{p_1}{1 + p_2 rc} - p_3 a \tag{10}$$

$$\frac{dr}{dt} = \frac{(cr)^2}{p_4 + (cr)^2} + p_5 - p_6 r \tag{11}$$

$$\frac{dc}{dt} = a_\tau - c. \tag{12}$$

The first equation describes the dynamics of ACTH release (a). It includes the key fact that CORT (c) inhibits the release of ACTH from corticotrophs by placing c in the denominator of the first term. This inhibitory action is rapid, so no time delay is included. CORT also increases the number of CORT receptors (r) expressed in the membrane of the corticotrophs. Thus, r is a dynamic variable, and c affects the speed at which r changes over time through the first term in the right hand side of Eq. 11. This is a saturating increasing function of c, and since c has an exponent greater than 1 it is called a *Hill function* with Hill coefficient of 2. Finally, a increases the release of CORT, but with a time delay of

τ (Eq. 12). Although only the last equation is a DDE, the equations are coupled and together form a DDE system.

DDEs have been used in several neuroendocrine applications in addition to ultradian glucocorticoid rhythms. They have been used in a model for the semi-circadian rhythm in prolactin secretion that occurs during the first half of pregnancy in rodents (2), in a model of ultradian rhythms in growth hormone secretion (43), and in the response of gonadotrophs to GnRH (56).

Partial differential equations

The final type of equation found in dynamic physiological models is the PDE. This would be used, for example, when spatial as well as temporal changes in a variable are included in the model. A good example is the *Hodgkin-Huxley cable equation*, which (along with the ODEs for the gating variables) describes the membrane potential along the length of an axon (24). The cable equation can be used to simulate the propagation of an action potential down an axon, and indeed was used in the seminal 1952 paper by Hodgkin and Huxley. It is:

$$C_{\mathrm{m}}\frac{\partial V}{\partial t}=\frac{\partial}{\partial x}\left(D\frac{\partial V}{\partial x}\right)+I_{\mathrm{app}}-I_{\mathrm{Na}}-I_{\mathrm{K}}-I_{l} \qquad (13)$$

where the single time derivative is replaced by partial derivatives for time and space (x) and the diffusion coefficient (D) includes the resistivity of the intracellular and extracellular media. PDE models are also often used to describe the diffusion of calcium in large cells such as neurons (24) and have been used to describe calcium dynamics in gonadotrophs (37). A PDE model was also used to describe the follicular selection process (8). The solution of PDEs requires analysis or numerical techniques that are more complex than those needed for ODEs, but many of the concepts discussed in the remainder of this article apply to both ODEs and to PDEs, so we focus on the simpler ODE models.

Equilibria and their Stability

Systems with a single stable equilibrium

One is often interested in long-term behavior. Mathematicians refer to this as the *asymptotic state* of the system, and the behavior at earlier times as the *transient behavior*. There is often a single asymptotic state, in which case the system is called *monostable*. If you drop an object onto the floor, then the asymptotic location is the floor, and the transient behavior is everything that happened before the object hit the floor. The system is monostable since there is only one floor, and gravity ensures that the object gets there. This asymptotic state is an *equilibrium* or *steady state* of the system, since once the object reaches the floor its position stops changing. To find the equilibrium or equilibria of a system of ODEs, it therefore makes sense to set all the time derivatives to 0.

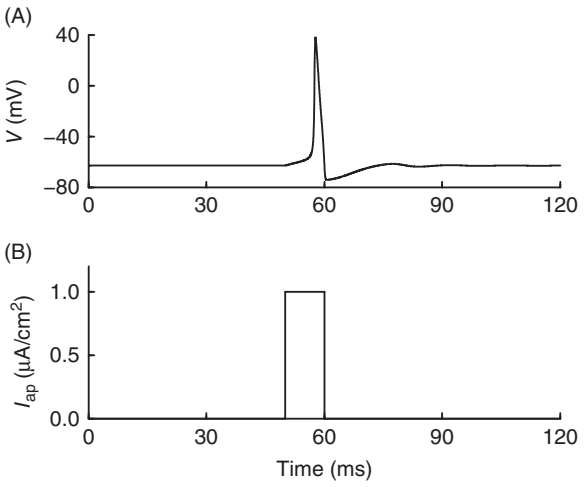

Figure 2 (A) With no applied current the Hodgkin-Huxley system is at equilibrium. (B) When a brief current pulse is applied an action potential is produced. The system returns to equilibrium after the pulse. The XPPAUT software package was used to numerically solve the equations in this and other figures. Codes can be downloaded from www.math.fsu.edu/~bertram/software/pituitary.

Doing this for the Hodgkin-Huxley equations, one obtains a set of four algebraic equations:

$$I_{\mathrm{Na}}+I_{\mathrm{K}}+I_{\mathrm{leak}}=I_{\mathrm{ap}} \qquad (14)$$

$$m=m_{\infty}(V) \qquad (15)$$

$$n=n_{\infty}(V) \qquad (16)$$

$$h=h_{\infty}(V). \qquad (17)$$

The solutions to these equations are the equilibria. For example, Figure 2 shows the voltage time course obtained by numerically solving the dynamic equations Eqs. 3 to 6. When the applied current is 0 the system has an equilibrium solution in which the voltage is about −64 mV (this could be found by solving the equilibrium equations Eqs. 14 to 17 with $I_{\mathrm{ap}}=0$). When the system is perturbed from rest with a short pulse of applied current (panel B) an action potential is produced (panel A). This is a transient response, and the system returns to rest shortly thereafter. The equilibrium is said to be *globally stable*, since the solution always returns there regardless of the size of the perturbation.

Bistable systems

Can there be more than one stable equilibrium? Not if the system of ODEs is linear. However, for nonlinear systems there can be two or more stable equilibria. In fact, it is often the case that physiological models are *bistable;* they have two stable equilibria. Such is the case, for example, in a model for long-term synaptic plasticity mediated by postsynaptic Ca^{2+}/Calmodulin-dependent protein kinase 2 (CamK2) (85). Activation of the kinase results in autophosphorylation, which if sufficiently large can put the enzyme into an active state

that persists after the stimulus (a high-frequency presynaptic impulse train) is removed. The activated state is stable, as is the original inactive state. The presynaptic impulse train simply moved the system from one stable equilibrium to the other. Bistability is also a key factor in a model of semi-circadian prolactin surges that occur during pregnancy in the rat. In this model, a brief mating stimulus moves a population of hypothalamic interneurons from an inactive state to an active state. The activated neurons inhibit dopamine neurons of the arcuate nucleus, which allows the prolactin surges to occur as long as the interneurons remain active (2). Bistability is also an important dynamic component of a model for synchronization of GnRH neuron activity (26) and a model for *in vivo* spike activity in phasically firing vasopressin neurons (7).

A nice illustration of a bistable system is the *genetic toggle switch*, which has been constructed in synthetic biology experiments (19). Here, one gene product represses the synthesis of another, and the reactions are mutual. This system can be described mathematically with the model:

$$\frac{dx}{dt} = \frac{\alpha_x}{1 + y^\beta} - x \tag{18}$$

$$\frac{dy}{dt} = \frac{\alpha_y}{1 + x^\gamma} - y \tag{19}$$

where x and y are the concentrations of the two repressors, α_x and α_y are the effective synthesis rate of the repressors, and β and γ are the cooperativities of repression. Notice that y is in the denominator of the synthesis rate for x (and *vice versa*), reflecting its role as a repressor. The equilibria of the model satisfy the algebraic equations:

$$x = \frac{\alpha_x}{1 + y^\beta} \tag{20}$$

$$y = \frac{\alpha_y}{1 + x^\gamma}. \tag{21}$$

Each of these equations is just a curve in the xy plane, and since they were derived by setting derivatives to 0 they are called *nullclines*. The first equation is the x nullcline and the second is the y nullcline. The nullclines are very useful in the mathematical analysis of two-dimensional or *planar* systems (65), but we focus here only on the fact that equilibria lie on both nullclines, so they can be found geometrically by plotting the two curves and looking for the intersections; *the equilibria are the intersections of the nullclines*.

Figure 3 shows the nullclines plotted in the xy plane (the x nullcline is black and the y nullcline is green). This plane is also the state space of the system (since it has the two dependent variables on the axes), and is referred to as the *phase plane*. From the figure, we see that there are three nulllcline intersections. How can this be, if the system only has two stable equilibria? It must be that one of the equilibria is unstable. That is, although it is a true equilibrium (if the initial values of x and y are equal to the x and y values of the nullcline intersection, then neither x nor y changes over

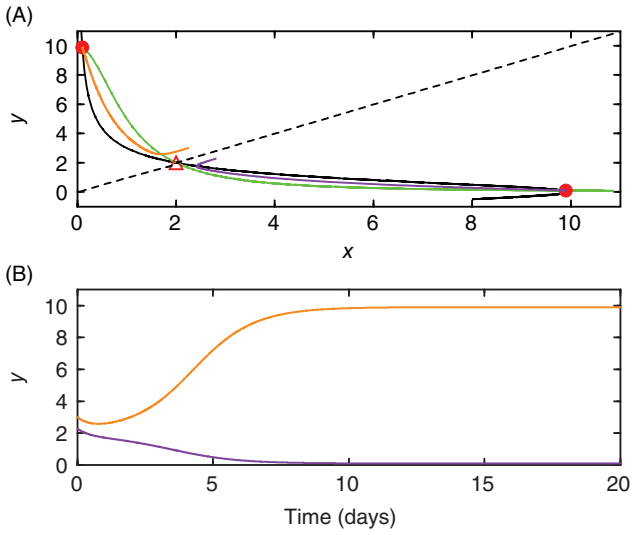

Figure 3 (A) Phase plane illustration of a bistable genetic toggle switch. The x nullcline (black), y nullcline (green), separatrix (dashed), equilibrium points (red circles and triangle), and two trajectories (orange and violet) are shown. (B) The time courses of the y variable for the two trajectories. One approaches the lower equilibrium while the other approaches the upper equilibrium. Parameter values are $\alpha_x = \alpha_y = 10$, $\beta = 2$, and $\gamma = 2$.

time), if a small perturbation is applied to the system it will usually move away from the unstable equilibrium to one of the stable equilibria. In Figure 3 the unstable equilibrium is represented by an open triangle, while the two stable equilibria are represented by closed circles.

For one of the stable equilibria (also called *stable nodes*) the x repressor dominates, and y is present only at a small concentration. For the other stable equilibrium the y repressor dominates, and x is present with a small concentration. This situation is similar to *competitive exclusion* in population dynamics, where two species competing in the same niche ultimately results in one species dominating the other and driving it to extinction. But how are the winner and the loser determined? What about the unstable equilibrium, does it have any importance? It turns out that the answer to the first question is related to the answer of the second. Since the unstable equilibrium (in which both repressors coexist at equal, but low, concentrations) is unstable, the real biological system would never be found in this state. This is because real systems have noise, and any amount of noise could drive the system away from the unstable equilibrium. So in this respect, the unstable equilibrium is unimportant. However, this equilibrium also holds the key to the question of which repressor ultimately dominates the other. The unstable equilibrium is a special type of equilibrium called a *saddle point*. There is a curve in the phase plane that connects to this point called the *stable manifold* of the saddle point (dashed curve in Fig. 3A). If the initial x and y values are such that the point lies on this stable manifold, then the system will be attracted to the saddle point, and not to one of the stable equilibria. In dynamical systems lingo, if the phase point starts on the stable manifold,

then it stays on the stable manifold and will be attracted to the saddle point (and reach it as $t \to \infty$). More importantly, the stable manifold of the saddle point is also the *separatrix* that divides the phase plane into two parts; all phase points (initial conditions) above the separatrix will evolve toward the stable equilibrium in which y dominates. All those below the separatrix evolve toward the stable equilibrium in which x dominates. (In this case, the separatrix is the line $y = x$, but in most other systems it is not linear.) The orange curve in Figure 3A is the path taken in the phase plane, called a *trajectory*, for a point starting above the stable manifold. The violet curve is a trajectory starting below the stable manifold. The portion of the plane above the separatrix is called the *basin of attraction* of the y-dominating equilibrium, while the portion below is the basin of attraction of the x-dominating equilibrium. So, the ultimate fate of this bistable system is determined by which basin of attraction the phase point starts in, that is, the initial values of x and y. Each of the stable steady states is *locally stable*, but not globally stable; if perturbed away from a stable steady state the system will return to that steady state, unless the perturbation is large enough to send the system into the basin of attraction of the other stable steady state.

The lower panel in Figure 3 shows the time courses of the y variable for the two trajectories shown in the top panel. Now time is represented explicitly (it is on the horizontal axis), while in the phase plane diagram in the top panel time is represented only implicitly through the orientation of the trajectories (toward the stable equilibria). Also, note that the y time course for the orange trajectory approaches 10, while that for the violet trajectory approaches a value near 0, just as in the phase plane diagram.

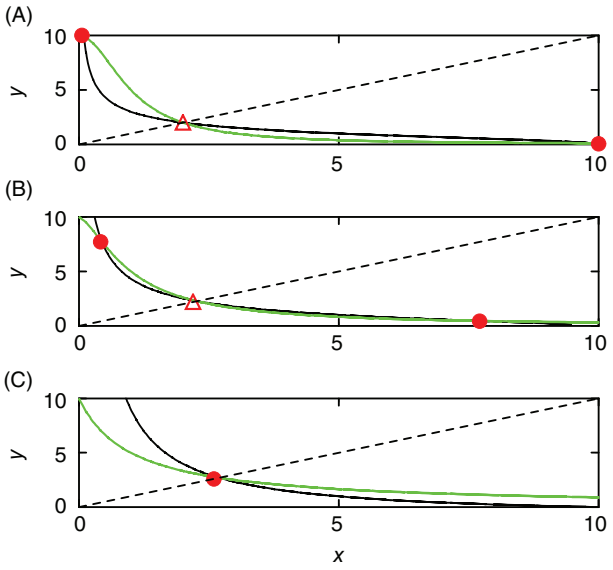

Figure 4 The x nullcine (black) and y nullcline (green) for the genetic toggle switch with $\alpha_x = \alpha_y = 10$ and $\beta = \gamma$. (A) $\beta = 2$, (B) $\beta = 1.5$, and (C) $\beta = 1$. The dashed curve is the line $y = x$ and equilibria are indicated by red circles or a triangle.

Bifurcations of Equilibria

The pitchfork bifurcation

The genetic toggle switch has three equilibria, reflecting the three intersections of the nullclines. What happens if we change the values of the parameters? Are there still three intersections? To check, and to make things simpler, we assume that the cooperativity of each repressor is the same, so $\beta = \gamma$. Then we can vary a single parameter, the cooperativity, and see what happens to the nullclines. Figure 4 shows the nullclines plotted for three different values of the cooperativity β. When $\beta = 2$, the original value, there are three intersections. When $\beta = 1.5$ both nullclines change, but there are still three intersections. It is clear that the nullclines are now closer together, as are the equilibria. When $\beta = 1$ the nullclines have crossed, so there is now a single intersection that occurs on the line $y = x$. Since this equilibrium is stable, the system has gone from being bistable to monostable. This is a big change: when the system was bistable one repressor dominated the other, while with the monostable system the two repressors coexist at equal concentrations. This is no longer a toggle switch, but more of a master diplomat. Such an extreme change in the system dynamics, where the number of equilbria changes, is called a *stationary bifurcation*.

The bifurcation in the genetic toggle switch was illustrated using a few values of the parameter β, and the bifurcation occurred for some value of β between 1 and 1.5. To get a better estimate of the bifurcation point we could keep changing β and look for the value when the three equilibria first coalesce into a single equilibrium. A better way is to use a *continuation method*, in which a parameter (called the *bifurcation parameter*) is varied in a continuous manner. Then the bifurcations can be found more precisely and with less work. Computer software exists for this, called AUTO (11), and this is included in the XPPAUT software package that is used to numerically integrate differential equations (13). AUTO uses the technique of numerical continuation to produce *bifurcation diagrams*, which show the number of equilibria and their stability for a range of values of the bifurcation parameter (60).

A bifurcation diagram for the genetic toggle switch is shown in Figure 5A. Here, the bifurcation parameter is the cooperativity β, ranging from 1 to 2. The vertical axis shows the y value of the equilibrium. For values of β near 1 there is a single equilibrium, whose y value declines somewhat as β increases. The curve is the y value for the set of equilibria. For values of β near 2 there are three equilibria. The lower and upper equilibria are stable, and represented with solid curves. The middle equilibrium is unstable, and represented with a dashed curve. As β is decreased from 2, the branches of stable equilibria approach each other, just as the stable equilibria approached each other in the phase plane diagram of Figure 4. When $\beta = 1.316$, the three equilibria coalesce. This is the stationary bifurcation point. There are several types of stationary bifurcations (65), but this one is perhaps the most

appropriately named: it is called a *pitchfork bifurcation*. This type of bifurcation was prominent in a study of coupling among pancreatic β cells (73).

The saddle-node bifurcation

Pitchfork bifurcations only occur in symmetric systems, and for this reason they are not very common. The genetic toggle switch model (Eqs. 18 and 19) is symmetric with the parameter values that we used, since the two equations are identical to each other when x and y are interchanged. This symmetry is easily broken by making $\alpha_x \neq \alpha_y$ or $\beta \neq \gamma$ (but we prefer to keep the cooperativities equal and use β as a bifurcation parameter). In Figure 5B we make a slight symmetry-breaking modification, using $\alpha_x = 9$ and $\alpha_y = 10$. The effect on the bifurcation diagram is dramatic. At low values of β, there is still a single stable equilibrium, but this branch never splits, instead continuing for the full range of β values. There is now a separate pair of branches that are born at $\beta \approx 1.45$. One branch is unstable and consists of saddle points. The other is stable and consists of stable nodes. The bifurcation is the point at which the saddle point branch and the node branch intersect and it has many names. It is sometimes called a *turning point*, or a knee, and sometimes even a nose! We will use the more mundane name of *saddle-node bifurcation*.

Unlike the pitchfork bifurcation, the saddle-node bifurcation requires no symmetry in the system, and for this reason is ubiquitous in the dynamics of physiological models [for example, (12, 26, 71)]. Because of the generality of this type of bifurcation it is termed a *generic bifurcation*.

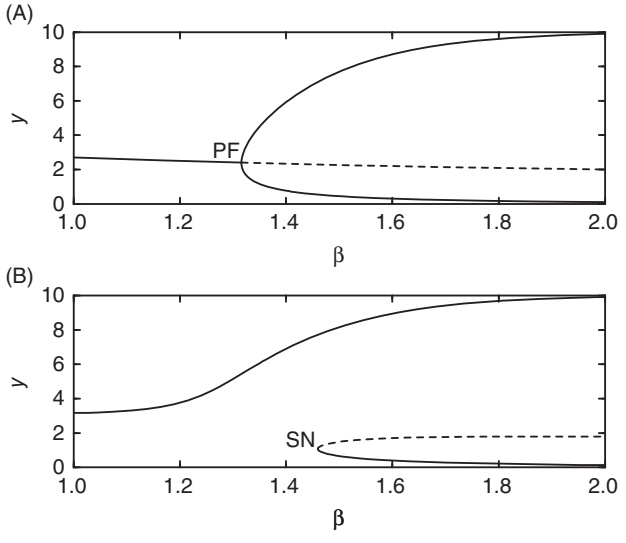

Figure 5 Bifurcation diagrams for the genetic toggle switch model with $\beta = \gamma$, $\alpha_y = 10$, and (A) $\alpha_x = 10$, or (B) $\alpha_x = 9$. PF, pitchfork bifurcation; SN, saddle-node bifurcation; solid curve, stable equilibria; dashed curve, unstable equilibria.

Oscillatory Systems

Oscillations are ubiquitous in the neuroendocrine system. One example is the pulsatile release of GnRH that is crucial for secretion of the gonadotropins luteinizing hormone and follicle-stimulating hormone by pituitary gonadotrophs (1, 27, 83). Another example is the ultradian pattern of glucocorticoid release, which is itself modulated with a circadian component (39). Of course, the estrous and menstrual cycles are also oscillations. Oscillations are also prevalent at the single cell level, such as Ca^{2+} oscillations in pituitary gonadotrophs and oscillations in the electrical activity of anterior pituitary cells (35, 64). The detailed mechanisms for these and other physiological oscillations vary considerably, but there are some common concepts that underlie them all. We consider a few of these here.

Slow or delayed negative feedback as a rhythmogenic mechanism

Perhaps the most prevalent mechanism for oscillations is slow or delayed negative feedback. To demonstrate that delayed negative feedback can lead to sustained oscillations, we use a mathematical model proposed for the semi-circadian secretion of prolactin that occurs in rodents during the first half of pregnancy (2). This twice-daily prolactin surge pattern can be induced in ovariectomized rats by cervical stimulation (18), and is important for the subsequent maternal behavior of the rat (20). The model builds on the well-known "short-loop feedback" of prolactin onto dopamine neurons of the arcuate nucleus (the tuberoinfundibular dopamine neurons, or TIDA neurons). Prolactin that is released by pituitary lactotrophs binds to receptors on the TIDA neurons and activates the JAK-STAT signaling pathway to increase the production and secretion of dopamine (18). This activation is delayed, however, since it requires the upregulation of tyrosine hydroxylase, which is a slow process (42). Why is this negative feedback? This is because the TIDA neurons release dopamine into the median eminence, and this dopamine inhibits lactotrophs, the very cells that activated the TIDA neurons. So from the point of view of the lactotrophs, the TIDA neurons provide negative feedback that is delayed due to the delay in activation of the TIDA neurons.

The mathematical model contains a differential equation for the secretion of prolactin (given by the variable PRL) that includes rapid inhibition by dopamine (given by the variable DA):

$$\frac{\mathrm{d}PRL}{\mathrm{d}t} = \frac{T_p}{1 + \mathrm{DA}^2} - q\mathrm{PRL}. \tag{22}$$

It also contains a DDE for DA, where the delay reflects the slow stimulatory action of PRL:

$$\frac{\mathrm{dDA}}{\mathrm{d}t} = T_d\left(1 + k_p\mathrm{PRL}_\tau^2\right) - q\mathrm{DA}. \tag{23}$$

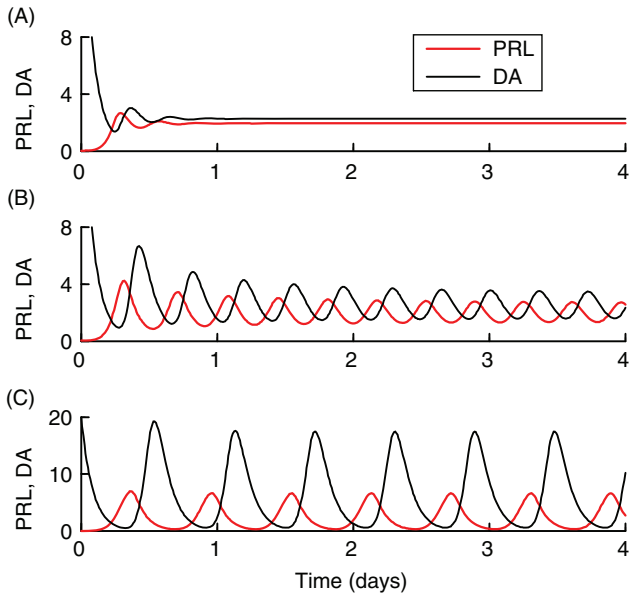

Figure 6 Sustained oscillations emerge in the prolactin model when the time delay is sufficiently large. (A) $\tau = 0.5$ h, (B) $\tau = 1.5$ h, and (C) $\tau = 3$ h. PRL and DA are dimensionless variables.

Notice that DA has an intrinsic drive of T_d in this model and that PRL adds to this, but with a time delay of τ. Figure 6 shows how this system responds with different values of the time delay (all other parameter values are as in Table 1). When the time delay is too short, for example, 0.5 h, the system only exhibits transient oscillations that die out as a stable equilibrium is reached (Fig. 6A). When the delay is increased to 1.5 h the oscillations are sustained, but the period is so short that on average there are more than two PRL surges per day (Fig. 6B). With a time delay of 3 h, however, oscillations still persist, but now have a period that is appropriate for the observed semi-circadian prolactin rhythm (Fig. 6C). Importantly, the oscillation period produced by the delayed negative feedback (~12 h) is much greater than the time delay (3 h). This is typical for oscillations driven by delayed negative feedback, and can make it hard to postulate a plausible delay mechanism without the aid of a mathematical model. That is, the period of the oscillation provides only a ballpark estimate of the time delay in the negative feedback, making it difficult to determine whether a proposed feedback loop can achieve the observed oscillation period without putting it into a model and trying it out.

Bifurcations involving oscillations

In the last example, there was a dramatic change in the dynamics when the time delay was increased from 0.5 to 1.5 h; the damped oscillations with $\tau = 0.5$ h became sustained with $\tau = 1.5$ h, and the stable equilibrium became unstable. These changes indicate that a *Hopf bifurcation* occurred for some critical value of τ between 0.5 and 1.5 h. This type of bifurcation is found over and over again in neuroendocrine models (4,12,26,57,71,82), and is the primary means through which sustained oscillations are born.

Another system exhibiting a Hopf bifurcation is the Hodgkin-Huxley model (Eqs. 3-8). Although this does not have an explicit time delay, oscillations are still possible since the negative feedback (the inactivation of Na^+ channels and activation of K^+ channels) is slow relative to the positive feedback (activation of Na^+ channels). In fact, the slow negative feedback is absolutely necessary for the production of action potentials. Figure 7A and B shows the Hodgkin-Huxley model with two pulses of applied current I_{ap}. Initially there is no applied current and the system is at a low-voltage equilibrium. At time $t = 100$ ms a long pulse of depolarizing current is applied that evokes an action potential followed by a few small damped oscillations. These are transient effects and the system returns to rest before the end of the current pulse. Since the equilibrium was not destabilized (the voltage returned to rest), and the oscillations are transient, there was no Hopf bifurcation. Later, however, when I_{ap} is stepped from 0 to 1.5 $\mu A/cm^2$ a train of action potentials is produced, and this tonic spiking continues as long as the current pulse is maintained.

The transition from stationary to sustained periodic behavior (also called a *limit cycle*) shown in Figure 7A and B is an indication that a Hopf bifurcation is nearby. A reasonable hypothesis is that it occurs for I_{ap} somewhere between 1 and 1.5 $\mu A/cm^2$. If this were the case, then as long as I_{ap} is past this bifurcation point, the solution would be periodic. To test this, we modify the applied current protocol so that during the second step I_{ap} is first increased from 0 to 1 $\mu A/cm^2$ and then increased to 1.5 $\mu A/cm^2$. If our hypothesis is correct, then the increase of applied current to 1.5 $\mu A/cm^2$ will cross the bifurcation point and start a limit cycle oscillation. However, we see in Figure 7C and D that this does not happen. Instead, there is a single action potential during the second pulse when I_{ap} is increased to 1 $\mu A/cm^2$, and then only small wiggles when it is increased further. What's going on here?

To understand this complex behavior, we need to do more than perform computer simulations; we need to do some analysis. That is, construct a bifurcation diagram. Figure 8A shows a diagram made using the same technique as that used in Figure 5, except now in addition to a *stationary branch* (consisting of equilibrium solutions, in black), there are periodic branches (for limit cycles, in red). For periodic branches we plot both the minimum and the maximum voltage of the oscillation, so a single branch of periodic solutions will be represented with two curves in the diagram. When $I_{ap} = 0$ there is a stable equilibrium, and as the applied current is increased this equilibrium remains stable at approximately the same voltage until $I_{ap} \approx 1.8$ $\mu A/cm^2$, where a Hopf bifurcation occurs and the equilibrium becomes unstable. But this is at odds with our hypothesis that the bifurcation was between 1 and 1.5 $\mu A/cm^2$. How can this be? It becomes clear when the periodic branch is traced out, starting at the Hopf bifurcation (HB_1). The branch opens up backward and is unstable (dashed red curves). This is called a *subcritical Hopf bifurcation,* in

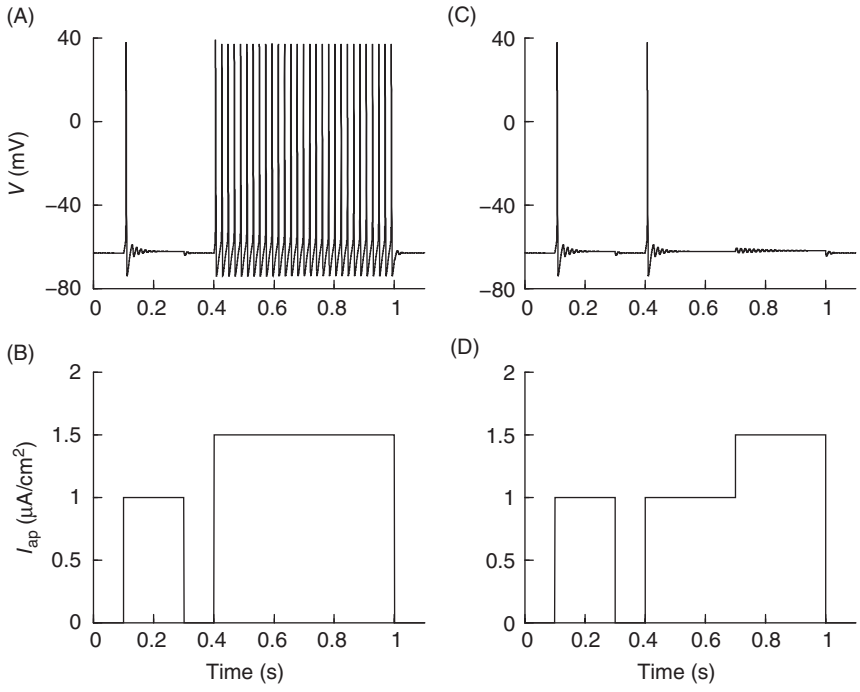

Figure 7 (A and B) A transient response is followed by a transition to tonic spiking with two consecutive current pulses of different sizes in the Hodgkin-Huxley model. (C and D) There is a very different response to the same final applied current if the approach is more gradual.

contrast to a *supercritical Hopf bifurcation* that would open with stable periodic solutions. The unstable periodic branch is complicated, opening backward, then going forward, and then backward again until it reaches the point labeled SNP. At this point the branch of unstable limit cycles turns to the right and forms a branch of stable limit cycles. This turning point is another bifurcation, called a *saddle-node of periodics* bifurcation. It occurs at $I_{ap} \approx 1.2$ μA/cm^2.

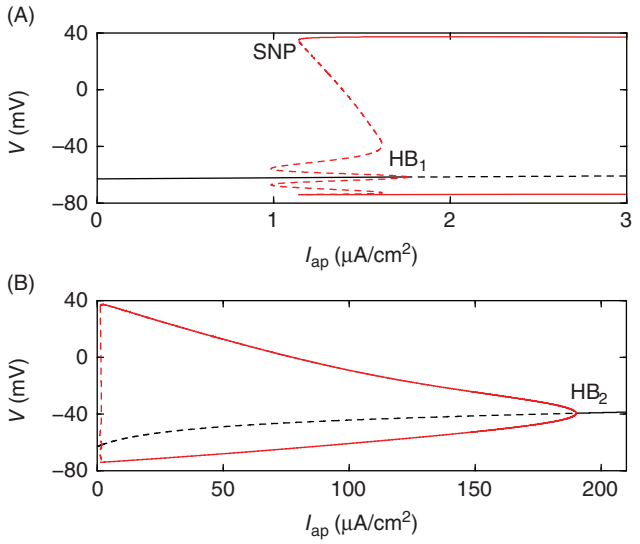

Figure 8 (A) Bifurcation diagram highlighting the subcritical Hopf bifurcation (HB_1) and the saddle-node of periodics bifurcation (SNP) in the Hodgkin-Huxley model. (B) Same diagram, but covering a larger range of the parameter. Highlights the supercritical Hopf bifurcation (HB_s). Stationary branches are in black and periodic branches are in red.

Now that we see the bifurcation structure of the system we can understand what happened in Figure 7. When $I_{ap} = 0$ the system is monostable with a single equilibrium. This is the resting potential. At $I_{ap} = 1$ μA/cm^2 the system is still monostable, so a pulse of current to this level may evoke transient spiking, but ultimately the system will return to rest. At $I_{ap} = 1.5$ μA/cm^2 however, the system is bistable with a stable equilibrium and a coexisting stable periodic solution. Which solution wins out? In Figure 7A and B the rapid increase from 0 to 1.5 μA/cm^2 moved the system far from its equilibrium and into the basin of attraction of the limit cycle, so there was a transition to tonic spiking. In contrast, in Figure 7C and D the rapid increase in current was to a value, 1 μA/cm^2, for which the system was still monostable, so only a transient spike was produced and the system then returned to equilibrium, as it must. The later increase of I_{ap} from 1 to 1.5 μA/cm^2 was not abrupt enough to move the system across the separatrix and into the basin of attraction of the limit cycle, so the system returned to equilibrium after a few transient subthreshold oscillations. Thus, bistability again comes into play, and we see that the way in which the system transitions from monostable to bistable, abruptly or gradually, determines the final outcome.

Subcritical Hopf bifurcations are common in neuroendocrine models, including models of GnRH neuron activity at three different time scales: bursting electrical activity (12), ultradian oscillations (26), and GnRH control of

ovulation (71). Another common dynamic structure is illustrated in Figure 8B. This shows the bifurcation diagram of the Hodgkin-Huxley model over a much wider range of values of the applied current than Figure 8A. Here, we see that the periodic branch of solutions that first became stable at the SNP extends to approximately 190 μA/cm^2, at which point it terminates at another Hopf bifurcation (HB_2). This time although the periodic branch again opens to the left at the bifurcation, the periodic solutions are born stable. This is an example of a supercritical Hopf bifurcation. Importantly, there is no bistability inherent in this type of Hopf bifurcation: to the left of the bifurcation the system is monostable with periodic solutions, and to the right it is monostable with equilibrium solutions. The branch of stable equilibria is at a much higher voltage than the stationary branch for I_{ap} near 0. In electrophysiology this is called *depolarization block*, since the resting voltage is so high that the negative feedback never turns off and thus there are no action potentials. This is, however, a very generic behavior that occurs whenever an oscillatory system is excited at a high level. Examples of this are seen in a model of glycolytic oscillations that produce insulin oscillations (4), a model for ultradian glucocorticoid oscillations (82), and a model for ultradian GnRH oscillations (26).

Stochastic Models

The models discussed thus far are all *deterministic*; if the differential equations are solved twice from the same set of initial conditions the output will be exactly the same. With *stochastic models* this is not the case. These models contain one or more random elements, with the randomness provided by pseudorandom number generator software that is present on all computers. Everything in biology is stochastic when examined on a fine scale. However, deterministic models often capture the essence of the behavior, and are simpler to analyze and solve on a computer. For this reason, deterministic models are usually the default choice. However, there are several reasons that one might use a stochastic model. One is that the system under consideration may have a low copy number. For example, if one is modeling gene expression the number of mRNA molecules may be small, so that fluctuations in the protein number would be large relative to the mean (so the coefficient of variation would be large). In this case, it would be best to use a *Markov model* in which state transitions are probabilistic. In contrast, if the number of mRNA molecules is large then the process could be well described by keeping track of the population mean, which would be a deterministic model. An excellent discussion of stochastic biological models is given in (16).

Another reason for using a stochastic model is that the system may contain either *intrinsic noise* or *extrinsic noise* that may play an important role in the system dynamics. If the system is a cell, the intrinsic noise could be due to fluctuations in the open state of an ion channel if the channel has a low copy number and has a large single-channel conductance. A good example is a model of the stochastic fluctuations in the number of open ATP-sensitive K^+ channels in a model of the pancreatic β cell, which provided an explanation for the different behaviors of single cells versus cells coupled together in an islet (61). It could also be due to factors in the cell that are not modeled explicitly, but introduce an important random element into the system, as in (66). Extrinsic noise could be due to synaptic input to a neuron, or random fluctuations in the hormone content acting on a cell. One recent example is a model of organized bursting electrical activity in response to suckling in a model of a population of oxytocin neurons (55). In this model, stochastic excitatory and inhibitory synaptic input is an essential ingredient in the coordinated network behavior.

To illustrate the effects that a small amount of noise can have on the system dynamics we use the Hodgkin-Huxley model again, but now add a term reflecting intrinsic noise to the voltage equation:

$$C_m \frac{dV}{dt} = I_{app} - I_{Na} - I_K - I_l - I_{noise} \quad (24)$$

where the noise is introduced as a stochastic current. This is expressed as:

$$I_{noise} = I_{noise}^{max} w/\sqrt{dt} \quad (25)$$

where I_{noise}^{max} is the maximum noise, and ω is a random process drawn from a normal distribution. Figure 9 shows the effect of adding a small amount of noise for two different values of the constant applied current. First, we consider $I_{app} = 1$ μA/cm^2, a case in which the deterministic system is monostable (Fig. 8). Without noise the system is at rest, but when a small amount of noise is added (arrow) sparse

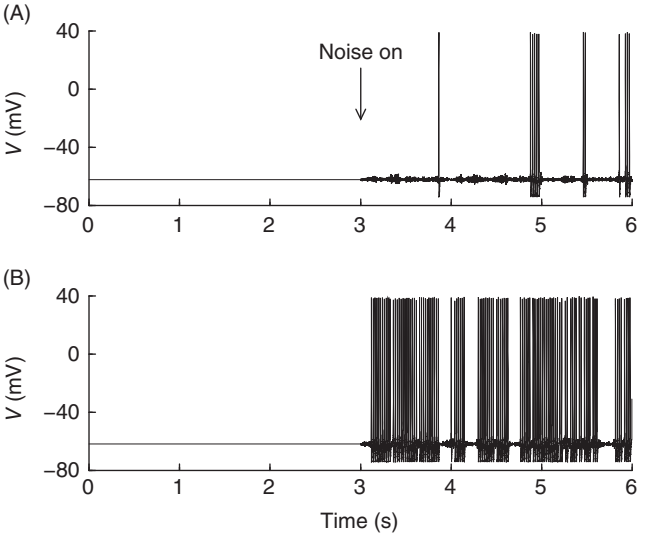

Figure 9 Hodgkin-Huxley time courses with and without noise. (A) $I_{app} = 1$ μA/cm^2. (B) $I_{app} = 1.5$ μA/cm^2.

clusters or bursts of action potentials are produced. Notice that the noise is quite small, as can be seen by the small fluctuations in the resting membrane potential between bursts. However, occasionally one of these noise-driven fluctuations pushes the system past the spike threshold, initiating a burst of action potentials. The apparently random timing of the bursts reflects the random nature of the noise, and the presence of a spike threshold amplifies the effect of the noise.

The lower panel of Figure 9 simulates the same thing, but now with a larger constant applied current, $I_{app} = 1.5\ \mu A/cm^2$. Recall that with this amount of applied current in the deterministic case the system is bistable between a resting steady state and a spiking periodic solution (Fig. 8). In the absence of noise, the resting membrane potential is almost identical to that with the smaller applied current in the top panel. However, when noise is added the system exhibits frequent and large bursts of spikes. In fact, the spike density is many times greater than it was when $I_{app} = 1\ \mu A/cm^2$, due partly to the existence of a stable periodic solution. We see that the 50% increase in constant applied current resulted in essentially no change in the system output in the absence of noise, but a much greater than 50% increase in the output (in terms of spike density) when noise is present. In this case, then, the presence of noise is absolutely vital for transducing a change in the input signal (the applied current) to an output response. This is achieved because the noise is acting on a system with two nonlinear features: a spike threshold and bistability between a steady state and a periodic solution. Thus, while system noise is typically considered to be a bad thing, it may actually be a key component of the signal transduction pathway. A more detailed discussion of the effects of noise on neural systems can be found in (14).

Systems with Multiple Time Scales

Most neuroendocrine systems vary with multiple time scales. For example, the production of an action potential in a GnRH neuron takes less than a hundred milliseconds. The action potentials are often clustered into bursts, with a period of 10 to 20 s. The bursts themselves are clustered into hourly pulses of activity. The pulse frequency varies throughout the ovarian cycle in females, providing the time scale of days. It can be quite challenging to construct models for multiscale systems such as this, so typically one is satisfied with a more limited model that spans one or two time scales. For example, several models have been developed for spiking and bursting activity in GnRH neurons (5, 17, 29, 30). These models include equations for membrane potential and various ionic currents, as well as for intracellular calcium. Other models only consider the potential mechanisms for the synchronization of electrical activity that results in hourly pulses of GnRH release, neglecting the detailed biophysics that occurs on much shorter time scales (26, 34). Finally, another set of models focus on the variation of pulse frequency during the ovarian cycle and the proestrus surge of activity (71, 76, 84). However, in spite of the challenges, modelers have learned a few tricks over the years to help cross time scales, and these approaches have been utilized in the analysis of several neuroendocrine models (12, 37, 49, 67, 76). In this section, we illustrate one prominent technique called *fast/slow analysis* that uses time scale separation to its advantage.

Relaxation oscillations

Perhaps the best-studied example of a system with multiple time scales is the van der Pol oscillator (74). This is a simple planar or two-dimensional system of ODEs in which one variable can be made much slower than the other, resulting in what are called *relaxation oscillations*. Models following this description are widely used in neuroscience and have been used as a simple representation for calcium dynamics in GnRH neurons (12) and as a simple representation of the hourly pulses of GnRH (76). For illustration, we consider the following planar system:

$$\frac{da}{dt} = a - a^3 - b \tag{26}$$

$$\frac{db}{dt} = \varepsilon\left(a + p_1 b + p_2\right) \tag{27}$$

where ε is a parameter that controls the speed of the variable b; b changes more slowly when ε is small.

The numerical solution of this "*a*-*b*" model is shown in Figure 10. When $\varepsilon = 1$ the time scales of the two variables are similar, so their time courses look similar (panel A). Since the system is planar we can gain insights from viewing the dynamics in the *ab*-phase plane (panel B). The a nullcline is cubic, $b = a - a^3$, while the b nullcline is linear, $b = -\frac{(a+p_2)}{p_1}$. There is a single equilibrium on the middle branch of the cubic nullcline, and this is unstable. Surrounding this unstable equilibrium is a stable limit cycle with counterclockwise orientation. We know from mathematical theory that this limit cycle must surround the equilibrium and we can determine the orientation without doing any computer simulation, but it is generally not possible to say more about the shape and location of the limit cycle in the phase plane without simulations. Thus, even in two dimensions the dynamics of nonlinear systems are largely inscrutable without the aid of the computer.

We now make the dynamics of b 20 times slower by setting $\varepsilon = 0.05$. This has no effect on either nullcline, but greatly increases the oscillation period, and also makes the shape of the b time course significantly different from that of the a time course (panel C). The a variable now quickly rises at the onset of the active phase of an oscillation and quickly falls at the end of the active phase, much like an action potential (simple relaxation models have been used to describe action potentials). This is referred to as a *square wave*. In contrast, b slowly rises during the active phase and slowly falls during the silent phase. This is referred to as a *saw tooth pattern*. The square wave time course of the fast variable and the saw tooth

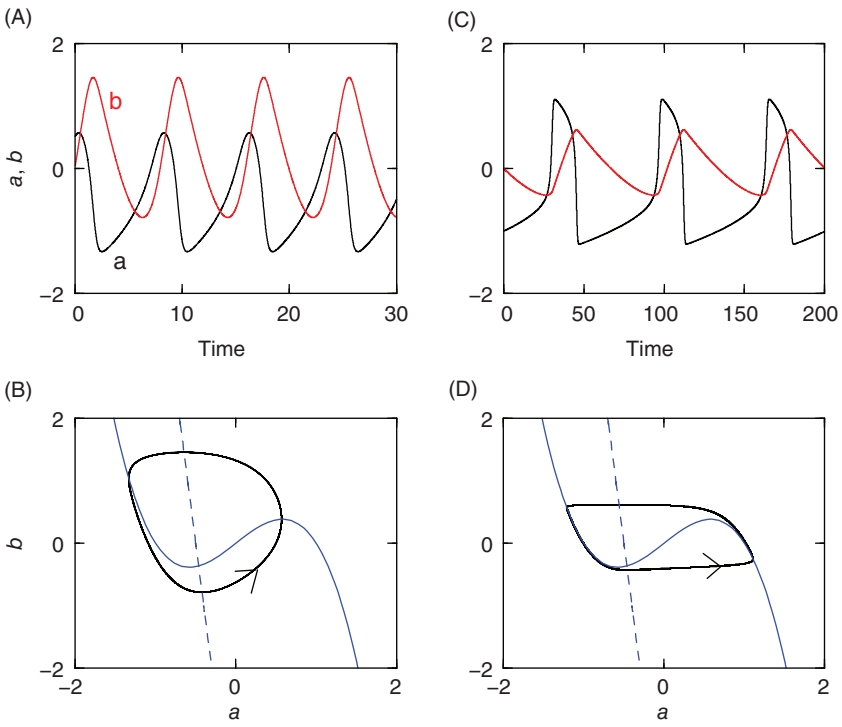

Figure 10 (A and C) Time course of the two variables in the planar relaxation oscillator. (B and D) Limit cycles in the phase plane, superimposed on the *x* nullcline (blue dashed) and the *y* nullcline (blue solid). Left: $\varepsilon = 1$. Right: $\varepsilon = 0.05$.

time course of the slow variable are characteristic features of a relaxation oscillation.

In the phase plane, the limit cycle trajectory rides along the two outer branches of the cubic *a* nullcline (the *fast nullcline*) during the active and silent phases and makes rapid transitions between them during the upstroke and downstroke of the active phase (panel D). In fact, one can determine the location of the limit cycle in the phase plane without doing any simulation at all: the trajectory moves along one branch of the fast nullcline until a knee is reached, at which time it moves almost horizontally to the other branch and the cycle continues. Thus, the separation of time scales allows us to view the two-dimensional dynamics as a sequence of one-dimensional motions (either along an outer branch or horizontally during rapid transitions). Yet, in spite of their apparent simplicity, relaxation oscillations posses some vary intricate dynamics near the Hopf bifurcation between stable equilibrium (and no limit cycle) and unstable equilibrium (with limit cycle), and these dynamics have been the focus of mathematical studies (10). So there is something to like for everyone.

Bursting electrical activity

Electrical bursting is ubiquitous in the nervous system, and it plays many roles from multifrequency information encoding to synaptic transmission (40). In the neuroendocrine system, bursting occurs in GnRH neurons (47), TIDA neurons (41), oxytocin neurons during suckling (31), and vasopressin neurons (31). Bursting also occurs in stimulated gonadotrophs, and in the spontaneous activity of many somatotrophs, lactotrophs, and corticotrophs (64). This is an inherently multiscale phenomenon since spikes are produced on one time scale and are clustered into bursts on a longer time scale. The complex multiscale dynamics of the oscillations have attracted mathematicians, who typically use fast/slow analysis to understand models of bursting. Indeed, an entire book has been written on models and analysis of bursting oscillations (9). Models of bursting in the neuroendocrine system are plentiful; models exist for bursting in GnRH neurons (5, 17), oxytocin neurons (28, 55), vasopressin neurons (7, 28, 44, 53), pituitary gonadotrophs (37), lactotrophs (67), somatotrophs (72), and corticotrophs (62).

In this section we use the simple "*s*-model" developed by Sherman (59) to illustrate how fast/slow analysis can be applied to bursting oscillations. This model serves as a template for the more complex models that have been developed for the various cell types and in many cases the approach used here can and has been applied to the more complex bursting models. The *s*-model consists of three variables, two of which are much faster than the third. The fast variables are the membrane potential (V) and the activation of delayed-rectifier K^+ channels (n). Activation of Ca^{2+} channels (m), which produce the upstroke of the action potential in this model, is so fast that it is approximated as being instantaneous. This is called a *quasi-equilibrium approximation*, and it is a frequently used device to reduce the dimensionality of the system. The slow

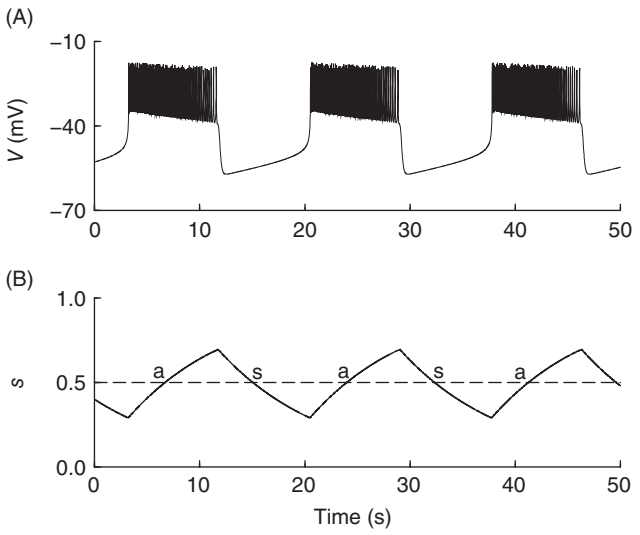

Figure 11 (A) Bursting electrical activity produced by the *s*-model. (B) The slow variable s has a saw tooth shape and for the same value of *s* the voltage may be in an active phase (*a*) or a silent phase (*s*), indicating bistability in the fast subsystem.

variable is the activation of a slowly activated K^+ conductance (s), which we refer to as K_s channels. The full system is described by the following ODEs:

$$\frac{dV}{dt} = -\left(I_{Ca} + I_K + I_{Ks} + I_{K(ATP)} + I_l\right)/C_m \quad (28)$$

$$\frac{dn}{dt} = \frac{n_\infty(V) - n}{\tau_n(V)} \quad (29)$$

$$\frac{ds}{dt} = \frac{s_\infty(V) - s}{\tau_s} \quad (30)$$

where $I_{Ca} = \bar{g}_{Ca} m_\infty(V)(V - V_{Ca})$, $I_K = \bar{g}_K n(V - V_K)$, $I_{Ks} = \bar{g}_{Ks} s(V - V_K)$, $I_{K(ATP)} = \bar{g}_{K(ATP)}(V - V_K)$, and $I_l = \bar{g}_l(V - V_l)$. This model is similar in form to the Hodgkin-Huxley model, but with a set of different ionic currents, including three types of K^+ currents. The time constant τ_s in the s ODE is large, which makes the s dynamics slow.

Figure 11 shows an example of bursting produced by the s model. During the spiking or active phase the s variable slowly rises, since the K_s channels are activated by the depolarization. The activated channels produce a hyperpolarizing current, which accumulates to the point where the system can no longer reach the spike threshold and the active phase terminates. The membrane potential then abruptly drops to a hyperpolarized level, leading to slow deactivation of the K_s channels (slow decline in s). As the associated hyperpolarizing current slowly declines, the membrane potential inches up toward the spike threshold. When this threshold is reached the silent phase is over and a new active phase begins.

It is instructive to notice a few points. First, the fast subsystem exhibits bistability, since the model cell can either be silent or active for the same value of s (illustrated by the dashed horizontal line in Figure 11B). Second, the s time course has a saw tooth pattern, just as the slow variable b in the relaxation oscillator (Fig. 10C). The V time course is in some ways similar to the fast variable a in the relaxation oscillator; during the silent phase it slowly rises. But it differs from the a time course in one important way; during the active phase it exhibits spiking rather than a plateau. Nevertheless, the similarities between the relaxation oscillator and the bursting oscillator suggest that one can apply a fast/slow analysis to bursting and gain insights similar to those gained with the relaxation oscillation (51).

The approach that has proven to be very effective in the analysis of bursting begins by thinking of the slow variable s as being so slow that it has no dynamics at all. That is, s is initially thought of as a parameter (rather than a variable) of the fast subsystem. Then, one investigates how the dynamics of the fast subsystem change with changes in s. An efficient way to do this is to create a bifurcation diagram, with s treated as the bifurcation parameter. The diagram in Figure 12A shows a z-shaped branch of equilibrium solutions of the fast subsystem (black). For each s value on the folded interval, s from approximately 0.3 to 1.3, there are three coexisting equilibria. However, only the lowest equilibrium is stable. The switchback points on the branch are a pair of saddle-node bifurcations. There is also a branch of stable periodic solutions (red) that emerges from a supercritical Hopf bifurcation. This branch terminates at a *homoclinic bifurcation*, where the period of the oscillation approaches infinity. While such a bifurcation, with infinite period, may seem strange for a biological model, we will see shortly that it does in fact explain a frequently observed behavior in bursting recordings. A key feature of the bifurcation diagram is that the stable stationary branch and the stable periodic branch overlap for a large range of s values. Thus, the fast subsystem

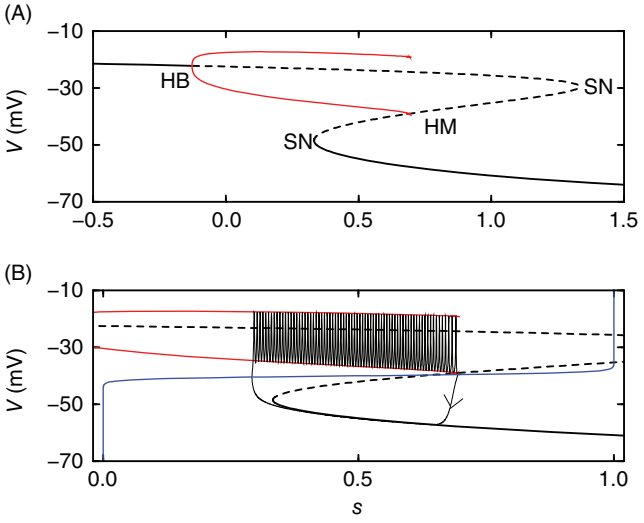

Figure 12 (A) Bifurcation diagram of the *V-n* fast subsystem for the s-model. Stationary (black) and periodic (red) branches are shown. SN, saddle-node; HB, Hopf; HM, homoclinic bifurcation. (B) Fast/slow analysis of *s*-model bursting. The *s* nullcline (blue) and burst trajectory are superimposed onto the *z* curve.

is bistable, as we deduced earlier. Hence, for any *s* value in the bistable interval the model cell could either be silent or spiking, depending on which basin of attraction it is in initially.

The next step in the fast/slow analysis is to add the *s* nullcline to the bifurcation diagram. At the same time, one thinks of the bifurcation diagram as a generalized *V* nullcline, which we call the *z* curve. This is done so as to reintroduce the *s* dynamics. That is, we now want to consider slow changes in *s* as well as the faster changes in *V* and *n*, and we want to use nullclines to predict these changes. We only show the *s* range from 0 to 1 in Figure 12B, since this is the physical range of values that this activation variable can take on.

The final step is to let *s* change in time according to its differential equation (Eq. 30), so that it is a variable again rather than a parameter. With the relaxation oscillator, the trajectory moved along the cubic fast nullcline until knees were reached, at which point it jumped to another branch (Fig. 10D). A similar thing happens with the bursting trajectory (superimposed on the *z* curve in Figure 12B). The generalized *V* nullcline is the equivalent of the fast nullcline, and during the silent phase the trajectory moves along the stable bottom branch. The motion is leftward because the trajectory is below the *s* nullcline and the *s* derivative is negative in this region. Thus, *s* declines during the silent phase, as we see in the *s* time course shown in Figure 11B. Once the knee (saddle-node bifurcation) is reached and the stable stationary branch ends, the trajectory has nowhere to go but up to the stable periodic (spiking) branch. This is the beginning of the active phase of the burst. Now that the trajectory is on the other side of the *s* nullcline it moves rightward as it spikes. Thus, *s* increases during the active phase, as in Figure 11B. The rightward spiking motion continues until the periodic branch ends at the homoclinic bifurcation, at which point the trajectory moves to the only remaining stable branch, which is now the bottom stationary branch of the *z* curve. This terminates the active phase and initiates a new silent phase.

What are the advantages to using this fast/slow analysis for bursting? There are many. First, it explains from a dynamic perspective many features of the burst. It tells us, for example, that the spiking should slow down during the active phase, since the fast subsystem is nearing an infinite-period homoclinic bifurcation. Indeed, this spike slowdown is evident in the bursting shown in Figure 11A. The analysis also tells us that the spikes should ride on a depolarized plateau, since the minimum voltage curve of the periodic branch is far above the bottom branch of the *z* curve. It tells us the range of parameter values where bursting will occur. If the *s* nullcline intersects the bottom branch of the *z* curve then the full system has a stable hyperpolarized equilibrium. That is, the model cell is at rest, with only transient spiking possible. If the *s* nullcline intersects the periodic branch of the *z* curve, then in many cases the system will spike continuously rather than burst. To ensure that the system bursts, then, the *s* nullcline must intersect the *z* curve between the lower saddle node and the homoclinic bifurcation. Another, more fundamental, requirement for bursting is that there must be bistability between a stationary branch of fast subsystem equilibria and a periodic spiking branch [unless there is more than one slow variable (3,52)]. Knowing these things makes it much easier for modelers to design models for bursting cells, and so even if the diagrams are not always shown in publications, they are often used when building and calibrating the model.

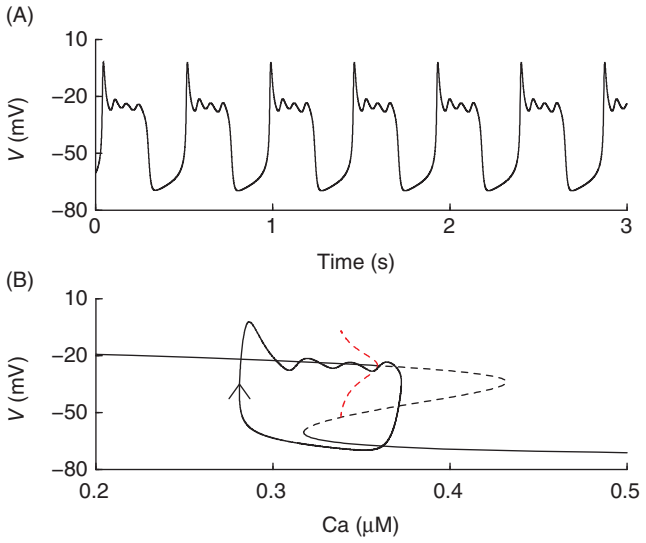

Figure 13 (A) Pseudoplateau bursting produced by a model of the pituitary lactotroph. Note the short duration and small spikes. (B) Standard fast/slow analysis of the pseudoplateau bursting. The periodic branch (red) is unstable.

Bursting in pituitary lactotrophs, somatotrophs, and corticotrophs is fundamentally different from bursting in gonadotrophs and most neurons. In these pituitary cells, the bursts are very short and the spikes have very small amplitude. An example with a lactotroph model (69) is shown in Figure 13A. The fast/slow analysis that works so well for the *s* model now runs into trouble. First of all, there is no stable periodic branch in the fast subsystem *z* curve, only a branch of unstable periodics (Fig. 13B). Equally as disturbing, the bursting trajectory does not follow the *z* curve very closely, raising the question of how useful the *z* curve is for this type of bursting. In recent years, great progress has been made in the development of analysis techniques for understanding this so-called *pseudoplateau bursting* (46, 49, 69, 77, 80). These techniques build on the fast/slow analysis discussed above, but require more sophisticated mathematical machinery.

Conclusion

The central aim of this overview was to describe some basic mathematical concepts used by modelers and some common dynamical motifs that are present in many neuroendocrine models. We have also pointed to publications where some of these motifs appear, although some have surely been missed. In the author's opinion, the field of mathematical neuroendocrinology is still in an early stage and there is great

potential for future developments. Mathematics has clearly had an impact on neuroendocrinology, both in the interpretation of data and in the design of experiments. Indeed, most of the modeling papers cited in this article were designed to answer specific biological questions. More surprisingly, neuroendocrinology has had an impact on mathematics. For example, pseudoplateau bursting in pituitary cells has spawned a series of papers involving sophisticated mathematical analysis (46, 48, 49, 63, 68-70, 77, 80), and has served as motivation for extensions in the theory of mixed-mode oscillations (78, 79). Mathematical modeling and neuroendocrinology have proven to be good for each other thus far.

Acknowledgement

The author's research on the neuroendocrine system is supported by NIH grant DK43200.

References

1. Belchetz PE, Plant TM, Nakai Y, Keogh EJ, Knobil E. Hypophysial responses to continuous and intermittent delivery of hypothalamic gonadotropin-releasing hormone. *Science* 202: 631-633, 1978.
2. Bertram R, Egli M, Toporikova N, Freeman ME. A mathematical model for the mating-induced prolactin rhythm of female rats. *Am J Physiol* 290: E573-E582, 2006.
3. Bertram R, Previte J, Sherman A, Kinard TA, Satin LS. The phantom burster model for pancreatic β-cells. *Biophys J* 79: 2880-2892, 2000.
4. Bertram R, Sherman A, Satin LS. Metabolic and electrical oscillations: Partners in controlling pulsatile insulin secretion. *Am J Physiol* 293: E890-E900, 2007.
5. Chen X, Iremonger K, Herbison AE, Kirk V, Sneyd J. Regulation of electrical bursting in a spatiotemporal model of a GnRH neuron. *Bull Math Biol* 75: 1941-1960, 2013.
6. Clarke IJ, Schlosser PM, Selgrade JF. Multiple stable periodic solutions in a model for hormonal control of the menstrual cycle. *Bull Math Biol* 65: 157-173, 2003.
7. Clayton TF, Murray AF, Leng G. Modelling the *in vivo* spike activity of phasically-firing vasopressin cells. *J Neuroendocrinol* 22: 1290-1300, 2010.
8. Clement F, Monniaux D. Multiscale modelling of ovarian follicular selection. *Prog Biophys Mol Biol* 113: 398-408, 2013.
9. Coombes S, Bressloff PC. *Bursting: The Genesis of Rhythm in the Nervous System*. Singapore: World Scientific, 2005.
10. Desroches M, Guckenheimer J, Krauskopf B, Kuehn C, Osinga HM, Wechselberger M. Mixed-mode oscillations with multiple time scales. *SIAM Rev* 54: 211-288, 2012.
11. Doedel EJ, Oldeman B. AUTO 07: Continuation and Bifurcation Software for Ordinary Differential Equations. Montreal, Canada: Concordia University, 2009.
12. Duan W, Lee K, Herbison AE, Sneyd J. A mathematical model of adult GnRH neurons in mouse brain and its bifurcation analysis. *J theor Biol* 276: 22-34, 2011.
13. Ermentrout B. *Simulating, Analyzing, and Animating Dynamical Systems: A Guide to xppaut for Researchers and Students*. Society for Industrial and Applied Mathematics, 2002.
14. Ermentrout GB, Terman DH. *Mathematical Foundations of Neuroscience*. Springer, 2010.
15. Erneux T. *Applied Delay Differential Equations*. Springer, 2009.
16. Fall CP, Marland ES, Wagner JM, Tyson JJ. Computational cell biology. In: *Interdisciplinary Applied Mathematics*. New York: Springer, 2002.
17. Fletcher PA, Li Y-X. An integrated model of electrical spiking, bursting, and calcium oscillations in GnRH neurons. *Biophys J* 96: 4514-4524, 2009.
18. Freeman ME, Kanyicska B, Lerant A, Nagy GM. Prolactin: Structure, function, and regulation of secretion. *Physiol Rev* 80: 1523-1631, 2000.
19. Gardner TS, Cantor CR, Collins JJ. Construction of a genetic toggle switch in *Escherichia coli*. *Nature* 403: 339-342, 2000.
20. Grattan DR. Behavioural significance of prolactin signalling in the central nervous system during pregnancy and lactation. *Reproduction* 123: 497-506, 2002.
21. Hille B. *Ion Channels of Excitable Membranes*. Sunderland, MA: Sinauer Associates, 2001.
22. Hodgkin AL, Huxley AF. A quantitative description of membrane current and its application to conduction and excitation in nerve. *J Physiol* 117: 500-544, 1952.
23. Izhikevich EM. *Dynamical Systems in Neuroscience; The Geometry of Excitability and Bursting*. Cambridge, MA: MIT Press, 2010.
24. Keener J, Sneyd J. *Mathematical Physiology 1: Cellular Physiology*. New York, NY: Springer, 2009.
25. Keener J, Sneyd J. *Mathematical Physiology II: Systems Physiology*. New York, NY: Springer, 2009.
26. Khadra A, Li Y-X. A model for the pulsatile secretion of gonadotropin-releasing hormone from synchronized hypothalamic neurons. *Biophys J* 91: 74-83, 2006.
27. Knobil E, Plant TM, Wildt L, Belchetz PE, Marshall G. Control of the rhesus monkey menstrual cycle: Permissive role of hypothalamic gonadotropin-releasing hormone. *Science* 207: 1371-1373, 1980.
28. Komendantov AO, Trayanova NA, Tasker JG. Somato-dendritic mechanisms underlying the electrophysiological properties of hypothalamic magnocellular neuroendocrine cells: A multicompartmental model study. *J Comput Neurosci* 23: 143-168, 2007.
29. LeBeau AP, van Goor F, Stojilkovic SS, Sherman A. Modeling of membrane excitability in gonadotropin-releasing hormone-secreting hypothalamic neurons regulated by Ca^{2+}-mobilizing and adenylyl cyclase-coupled receptors. *J Neurosci* 20: 9290-9297, 2000.
30. Lee K, Duan W, Sneyd J, Herbison AE. Two slow calcium-activated afterhyperpolarization currents control burst firing dynamics in gonadotropin-releasing hormone neurons. *J Neurosci* 30: 6214-6224, 2010.
31. Leng G, Brown CH, Russell JA. Physiological pathways regulating the activity of magnocellular neurosecretory cells. *Prog Neurobiol* 57: 625-655, 1999.
32. Leng G, MacGregor DJ. Mathematical modeling in neuroendocrinology. *J Neuroendocrinol* 20: 713-718, 2008.
33. Li Y-X, Keizer J, Stojilkovic SS, Rinzel J. Ca^{2+} excitability of the ER membrane: An explanation for IP_3-induced Ca^{2+} oscillations. *Am J Physiol* 269: C1079-C1092, 1995.
34. Li Y-X, Khadra A. Robust synchroniy and rhythmogenesis in endocrine neurons via autocrine regulations in vitro and in vivo. *Bull Math Biol* 70: 2103-2125, 2008.
35. Li Y-X, Rinzel J, Keizer J, Stojilkovic SS. Calcium oscillations in pituitary gonadotrophs: Comparison of experiment and theory. *Proc Natl Acad Sci U S A* 91: 58-62, 1994.
36. Li Y-X, Rinzel J, Vergara L, Stojilkovic SS. Spontaneous electrical and calcium oscillations in unstimulated pituitary gonadotrophs. *Biophys J* 69: 58-62, 1995.
37. Li Y-X, Stojilkovic SS, Keizer J, Rinzel J. Sensing and refilling calcium stores in an excitable cell. *Biophys J* 72: 1080-1091, 1997.
38. Liang Z, Chen L, McClafferty H, Lukowski R, MacGregor D, King JT, Rizzi S, Sausbier M, McCobb DP, Knaus H-G, Ruth P, Shipston MJ. Control of hypothalamic-pituitary-adrenal stress axis activity by the intermediate conductance calcium-activated potassium channel, SK4. *J Physiol* 589: 5965-5986, 2011.
39. Lightman SL, Conway-Campbell BL. The critical role of pulsatile activity of the HPA axis for continuous dynamic equilibration. *Nat Rev Neurosci* 11: 710-718, 2010.
40. Lisman JE. Bursts as a unit of neural information: Making unreliable synapses reliable. *Trends Neurosci* 20: 38-43, 1997.
41. Lyons DJ, Horjales-Araujo E, Broberger C. Synchronized network oscillations in rat tuberoinfundibular dopamine neurons: Switch to tonic discharge by thyrotropin-releasing hormone. *Neuron* 65: 217-229, 2010.
42. Ma FY, Grattan DR, Goffin V, Bunn SJ. Prolactin-regulated tyrosine hydroxylase activity and messenger ribonucleic actid expression in mediobasal hypothalamic cultures: The differential role of specific protein kinases. *Endocrinology* 146: 93-102, 2005.
43. MacGregor DJ, Leng G. Modelling the hypothalamic control of growth hormone secretion. *J Neuroendocrinol* 17: 788-803, 2005.
44. MacGregor DJ, Leng G. Phasic firing in vasopressin cells: Understanding its functional significance through computational models. *PLoS Comput Biol* 8(10): e1002740, 2012.
45. MacGregor DJ, Leng G. Spike triggered hormone secretion in vasopressin cells; a model investigation of mechanism and heterogeneous population function. *PLoS Comput Biol* 9(8): e1003187, 2013.
46. Nowacki J, Mazlan S, Osinga HM, Tsaneva-Atanasova K. The role of large-conductance calcium-activated K^+ (BK) channels in shaping bursting oscillations of a somatotroph cell model. *Physica D* 239: 485-493, 2010.
47. Nunemaker CS, Straume M, DeFazio RA, Moenter SM. Gonadotropin-releasing hormone neurons generate interacting rhythms in multiple time domains. *Endocrinology* 144: 823-831, 2003.
48. Osinga HM, Sherman A, Tsaneva-Atanasova K. Cross-currents between biology and mathematics: The codimension of pseudo-plateau bursting. *Discret Contin Dyn S* 32: 2853-2877, 2012.

49. Osinga HM, Tsaneva-Atanasova K. Dynamics of plateau bursting depending on the location of its equilibrium. *J Neuroendocrinol* 22: 1301-1314, 2010.
50. Press WH, Teukolsky SA, Vetterling WT, Flannery BP. *Numerical Recipes: The Art of Scientific Computing*. Cambridge: Cambridge University Press, 2007.
51. Rinzel J, Ermentrout B. Analysis of neural excitability and oscillations. In: Koch C, Segev I, editors. *Methods in Neuronal Modeling: From Ions to Networks*. Cambridge, MA: MIT Press, 1998, pp. 251-292.
52. Rinzel J, Lee YS. Dissection of a model for neuronal parabolic bursting. *J Math Biol* 25: 653-675, 1987.
53. Roper P, Callaway J, Armstrong W. Burst initiation and termination in the phasic vasopressin cells of the rat supraoptic nucleus: A combined mathematical, electrical, and calcium fluorescence study. *J Neurosci* 24: 4818-4831, 2004.
54. Roper P, Callaway J, Shevchenko T, Teruyama R, Armstrong W. AHP's, HAP's and DAP's: How potassium currents regulate the excitability of rat supraoptic neurones. *J Comput Neurosci* 15: 367-389, 2003.
55. Rossoni E, Feng J, Tirozzi G, Brown D, Leng G, Moos F. Emergent synchronous bursting of oxytocin neuronal network. *PLoS Comput Biol* 4: e1000123, 2008.
56. Scullion S, Brown D, Leng G. Modelling the pituitary response to luteinizing hormone-releasing hormone. *J Neuroendocrinol* 16: 265-271, 2004.
57. Selgrade JF. Bifurcation analysis of a model for hormonal regulation of the menstrual cycle. *Math Biosci* 225: 108-114, 2010.
58. Selgrade JF, Harriss LA, Pasteur RD. A model for hormonal control of the menstrual cycle: Structural consistency but sensitivity with regard to data. *J theor Biol* 260: 572-580, 2009.
59. Sherman A. Contributions of modeling to understanding stimulus-secretion coupling in pancreatic β cells. *Am J Physiol* 271: E362-E372, 1996.
60. Sherman A. Dynamical systems theory in physiology. *J Gen Physiol* 138: 13-19, 2011.
61. Sherman A, Rinzel J, Keizer J. Emergence of organized bursting in clusters of pancreatic β-cells by channel sharing. *Biophys J* 54: 411-425, 1988.
62. Shorten PR, Robson AB, McKinnon AE, Wall DJN. CRH-induced electrical activity and calcium signaling in pituitary corticotrophs. *J theor Biol* 206: 395-405, 2000.
63. Stern JV, Osinga HM, LeBeau A, Sherman A. Resetting behavior in a model of bursting in secretory pituitary cells: Distinguishing plateaus from pseudo-plateaus. *Bull Math Biol* 70: 68-88, 2008.
64. Stojilkovic SS, Tabak J, Bertram R. Ion channels and signaling in the pituitary gland. *Endocr Rev* 31: 845-915, 2010.
65. Strogatz SH. *Nonlinear dynamics and chaos: With applications to physics, biology, chemistry, and engineering*. Boulder, CO: Westview Press, 2001.
66. Tabak J, Tomaiuolo M, Gonzalez-Iglesias AE, Milescue LS, Bertram R. Fast-activating voltage- and calcium-dependent potassium (BK) conductance promotes bursting in pituitary cells: A dynamic clamp study. *J Neurosci* 31: 16855-16863, 2011.
67. Tabak J, Toporikova N, Freeman ME, Bertram R. Low dose of dopamine may stimulate prolactin secretion by increasing fast potassium currents. *J Comput Neurosci* 22: 211-222, 2007.
68. Teka W, Tabak J, Bertram R. The relationship between two fast/slow analysis techniques for bursting oscillations. *Chaos* 22: e043117, 2012.
69. Teka W, Tabak J, Vo T, Wechselberger M, Bertram R. The dynamics underlying pseudo-plateau bursting in a pituitary cell model. *J Math Neurosci* 1: 12, 2011.
70. Teka W, Tsaneva-Atanasova K, Bertram R, Tabak J. From plateau to pseudo-plateau bursting: Making the transition. *Bull Math Biol* 73: 1292-1311, 2010.
71. Tien JH, Lyles D, Zeeman ML. A potential role of modulating inositol 1,4,5-trisphosphate receptor desensitization and recovery rates in regulating ovulation. *J theor Biol* 232: 105-117, 2005.
72. Tsaneva-Atanasova K, Sherman A, Van Goor F, Stojilkovic SS. Mechanism of spontaneous and receptor-controlled electrical activity in pituitary somatotrophs: Experiments and theory. *J Neurophysiol* 98: 131-144, 2007.
73. Tsaneva-Atanasova K, Zimliki CL, Bertram R, Sherman A. Diffusion of calcium and metabolites in pancreatic islets: Killing oscillations with a pitchfork. *Biophys J* 90: 3434-3446, 2006.
74. van der Pol B, van der Mark J. The heartbeat considered as a relaxation oscillation, and an electrical model of the heart. *Phil Mag* 6: 763-775, 1928.
75. Van Goor F, Li Y-X, Stojilkovic SS. Paradoxical role of large-conductance calcium-activated K^+ (BK) channels in controlling action potential-driven Ca^{2+} entry in anterior pituitary cells. *J Neurosci* 21: 5902-5915, 2001.
76. Vidal A, Clement F. A dynamical model for the control of the gonadotropin-releasing hormone neuroscretory system. *J Neuroendocrinol* 22: 1251-1266, 2010.
77. Vo T, Bertram R, Tabak J, Wechselberger M. Mixed mode oscillations as a mechanism for pseudo-plateau bursting. *J Comput Neurosci* 28: 443-458, 2010.
78. Vo T, Bertram R, Wechselberger M. Bifurcations of canard-induced mixed mode oscillations in a pituitary lactotroph model. *Discret Contin Dyn S* 32: 2879-2912, 2012.
79. Vo T, Bertram R, Wechselberger M. Multiple geometric viewpoints of mixed mode dynamics associated with pseudo-plateau bursting. *SIAM J Appl Dyn Syst* 12: 789-830, 2013.
80. Vo T, Tabak J, Bertram R, Wechselberger M. A geometric understanding of how fast activating potassium channels promote bursting in pituitary cells. *J Comput Neurosci* 36: 259-278, 2014.
81. Walker JJ, Spiga F, Waite E, Zhao Z, Kershaw Y, Terry JR, Lightman SL. The origin of glucocorticoid hormone oscillations. *PLoS Biol* 10(6): e1001341, 2012.
82. Walker JJ, Terry JR, Lightman SL. Origin of ultradian pulsatility in the hypothalamic-pituitary-adrenal axis. *Proc R Soc B* 277: 1627-1633, 2010.
83. Wildt L, Hausler A, Marshall G, Hutchison JS, Plant TM, Belchetz PE, Knobil E. Frequency and amplitude of gonadotropin-releasing hormone stimulation and gonadotropin secretion in the rhesus monkey. *Endocrinology* 109: 376-385, 1981.
84. Zeeman ML. Resonance in the menstrual cycle: A new model of the LH surge. *Reprod Biomed Online* 7: 295-300, 2003.
85. Zhabodinsky AM. Bistability in the Ca^{2+}/calmodulin-dependent protein kinase-phosphatase system. *Biophys J* 79: 2211-2221, 2000.